Journal of Chromatography A, 1217 (2010) 4713–4722

Contents lists available at ScienceDirect

Journal of Chromatography A

journal homepage: www.elsevier.com/locate/chroma

Statistical analysis of packed beds, the origin of short-range disorder, and its impact on eddy dispersion

Siarhei Khirevich [a], Anton Daneyko [a], Alexandra Höltzel [a], Andreas Seidel-Morgenstern [b], Ulrich Tallarek [a,*]

[a] Department of Chemistry, Philipps-Universität Marburg, Hans-Meerwein-Strasse, 35032 Marburg, Germany
[b] Max-Planck-Institut für Dynamik komplexer technischer Systeme, Sandtorstrasse 1, 39106 Magdeburg, Germany

ARTICLE INFO

Article history:
Received 29 March 2010
Received in revised form 3 May 2010
Accepted 7 May 2010
Available online 19 May 2010

Keywords:
Packed beds
Packing method
Ordered packing
Random packing
Disorder
Degree of heterogeneity
Microstructure
Statistical analysis
Voronoï tessellation
Voronoï volume distribution
Eddy dispersion
Direct numerical simulation
Lattice-Boltzmann method
High-performance computing

ABSTRACT

We quantified the microstructural disorder of packed beds and correlated it with the resulting eddy dispersion. For this purpose we designed a set of bulk (unconfined) monodisperse random sphere packings with a systematic, protocol-dependent degree of microstructural heterogeneity, covering a porosity range from the random-close to the random-loose packing limit ($\varepsilon = 0.366$–0.46). With the precise knowledge of particle positions, size, and shape we conducted a Voronoï tessellation of all packings and correlated the statistical moments of the Voronoï volume distributions (standard deviation and skewness) with the porosity and the protocol-dependent microstructural disorder. The deviation of the Voronoï volume distributions from the delta function of a crystalline packing describes the origin of short-range disorder of the investigated random packings. Eddy dispersion was simulated over a wide range of reduced velocities ($0.5 \leq \nu \leq 750$) and analyzed with the comprehensive Giddings equation. Transient dispersion was found to correlate with the spatial scales of heterogeneity in the packings. The analysis of short-range disorder based on the Voronoï volume distributions revealed a strong correlation with the short-range interchannel contribution to eddy dispersion, whereas transchannel dispersion was relatively little affected. The presented approach defines a strictly scientific route to the key morphology–transport relationships of current and future chromatographic supports, including their morphological reconstruction, statistical analysis, and the correlation with relevant transport phenomena. It also guides us in our understanding, comparison, and optimization of the diverse packing algorithms and protocols used in simulations and experimental studies.

1. Introduction

The properties of a wide variety of materials, including liquids, glasses, crystals, and granular media, depend on the way particles pack and arrange [1]. One of the scientists who first investigated the microscopic nature of granular media was Bernal [2–4], who in a series of papers about the "structure of liquids" reported some of the most important features of the structural organization of disordered sphere packings. Bernal originally used random packings of ball bearings to study the structure of liquids and he coined the term 'random-close packing' to describe the densest random arrangement of spheres. Indeed, the filling of containers with balls is among the oldest physical puzzles known to scientists [5]. Apart from its mathematical significance, this problem has found applications in modern science related, e.g., to jamming in granular media, compaction of colloids, the structure of liquids, and the glass transition [6]. Despite the progress made in developing a statistical mechanics for such systems [7], the definition of jammed states and the characterization of their randomness are still intensively discussed [8–13].

In chromatography we have accepted to "jam-pack" columns by a slurry packing process that experience has told us to be most appropriate in terms of the traditionally measured (post-column) separation efficiency [14,15]. The packing process involves several, often strongly interrelated, parameters, among them the physicochemical properties of the stationary-phase particles, interparticle forces, slurry preparation, the application of pressure and ultrasound, as well as the coupled stress–strain-flow behavior [16]. Owing to the difficulty in probing the packing microstructure systematically as a function of all relevant process parameters, column packing and consolidation are largely treated phenomenologically and considered an art rather than a science. Although at present the packing process cannot be approached comprehensively by simulations, recent progress in our understanding and modeling of the dynamic behavior of

* Corresponding author. Tel.: +49 6421 28 25727; fax: +49 6421 28 22124.
E-mail address: tallarek@staff.uni-marburg.de (U. Tallarek).
URL: http://www.uni-marburg.de/fb15/ag-tallarek (U. Tallarek).

0021-9673/$ – see front matter © 2010 Elsevier B.V. All rights reserved.
doi:10.1016/j.chroma.2010.05.019

particulate systems originates from discrete particle simulation [17,18].

The density or particle volume fraction ρ of random sphere packings falls between $\rho \sim 0.55$ and $\rho \sim 0.64$, values which are commonly referred to as the random-loose-packing (RLP) and random-close-packing (RCP) limit, respectively [11,19–22]. In chromatography, the density of a column packing is more often described by the interparticle void fraction or interparticle porosity $\varepsilon = 1 - \rho$. Stable column packings can vary up to 15% in their interparticle porosities, depending on the packing parameters. Moreover, a given interparticle porosity is just a macroscopic value that may apply to a large number of columns with very different packing microstructures. The latter, however, determine the individual structure–transport relationships that govern hydrodynamic dispersion in and ultimately the separation efficiency of any packed column.

Packing microstructures are commonly classified as "more homogeneous" or "more heterogeneous". These intuitive, qualitative labels are usually based on column performance. Experimentally, it would be desirable to generate packings with a known and controllable degree of heterogeneity. However, this requires a sound scientific quantification of the degree of heterogeneity of the underlying, individual packing microstructure. An adequate quantification of the disorder (or microstructural degree of heterogeneity) in different packings, which could have the same packing density ρ or interparticle porosity ε, and a strong and sensitive correlation to the experimentally observable dispersion, has not yet been demonstrated.

Detailed three-dimensional numerical simulations of flow and transport in sphere packings are particularly suited to the challenge of investigating the central structure–transport relationships in chromatographic media, because this approach allows to systematically study relevant parameters, such as the shape and average size of the particles, the particle size distribution, inter- and intraparticle porosities, as well as the column dimensions and cross-sectional geometry [23–43]. Transient dispersion can be recorded easily, thereby quantifying time and length scales required for the attainment of asymptotic dispersion behavior and providing correlations for the dependence of dispersion on the mobile phase velocity. Because all dispersion data are referenced to a particular packing microstructure and are unbiased by extra-column contributions, the numerical simulations approach establishes a systematic route towards quantitative structure–transport relationships. Further, statistical information about the structure of the simulated packings can be collected, because position, size, and usually also the shape of the particles are known. However, the microstructures of computer-generated idealized random packings are protocol-dependent, just as packing density and column performance depend on the precise packing protocol in chromatographic practice [8,40]. Thus, any structure–transport analysis should be accompanied by a suitable statistical analysis of the employed packed beds. This will allow to compare and optimize the protocols for simulated as well as experimental packings, e.g., with respect to dispersion.

In the present study we apply a statistical and hydrodynamic analysis to packed beds to correlate disorder with dispersion. We employ Voronoï tessellation and use the distribution of Voronoï volumes to quantify the degree of heterogeneity of a packing. This method permits to explicitly capture the disorder of packed beds in the form of quantitative scalar measures. We demonstrate the great potential of this approach for a well-designed set of computer-generated bulk, random packings of monosized hard spheres with "more homogeneous" and "more heterogeneous" microstructures, covering packing densities from the RLP to the RCP limit, and their asymptotic longitudinal dispersion coefficients simulated over a wide range of mobile phase velocities. To our knowledge, this is the first report that sensitively correlates the actual disorder of packed beds with the measurable dispersion in packed beds, using Voronoï volume distributions as a suitable statistical measure.

2. Generation of packed beds

Experience tells us that both packing density or porosity and packing procedure affect dispersion. We therefore generated a set of bulk packings (which mimic infinitely wide, randomly packed beds without walls) with packing (interparticle) porosities ε from the RCP to the RLP limit and a systematically varied degree of heterogeneity.

Computationally, isotropic random monosized hard-sphere packings with periodic boundary conditions and dimensions of approximately $10d_p \times 10d_p \times 70d_p$ (where d_p is the sphere diameter) were successfully reproduced using a modified Jodrey–Tory (JT) algorithm [44]. The realized packing dimensions are sufficient for performing both statistical analysis of packing microstructure and simulations of hydrodynamic dispersion within the void space of a packing. The JT algorithm can be classified as a 'collective rearrangement' method. It starts from a random distribution of n sphere (particle) centers in a simulation box of volume V_{box}. Sphere overlap is typical in the initial configuration. The value of n is calculated from the targeted (final) packing porosity ε_{fin}, V_{box}, and the final sphere diameter $d_{p,fin}$ as

$$\varepsilon_{fin} = 1 - \left(\frac{n\pi d_{p,fin}^3}{6V_{box}} \right). \quad (1)$$

Each iteration of the algorithm includes (i) the search of the two particle centers C_1 and C_2 with minimum pair-wise distance $d_{p,min}$, where $d_{p,min}$ defines the maximal sphere diameter at which no overlap occurs in the current packing configuration with corresponding packing porosity $\varepsilon_{min} = 1 - (n\pi d_{p,min}^3/6V_{box})$; and (ii) the symmetrical spreading apart of these two particle center positions along a line C_1C_2 up to a new distance ($d_{p,max}$) according to the following equation:

$$d_{p,max} = d_{p,min} \left(1.0 + \alpha \log_{10} \left(\frac{d_{p,fin}}{d_{p,min}} \right) \right). \quad (2)$$

As $d_{p,min}$ asymptotically approaches $d_{p,fin}$ (Eq. (2)), ε_{min} approaches ε_{fin} (Eq. (1)). The algorithm exits when the condition $\varepsilon_{min} < 1.001\varepsilon_{fin}$ is satisfied. The constant α in Eq. (2) defines the magnitude of each displacement of centers C_1 and C_2, i.e., higher values of α cause larger displacements.

The JT algorithm produces geometrically jammed, but mechanically unstable sphere packings, because interparticle forces are not considered. On the other hand, the JT algorithm has the following advantages: (i) the porosity and degree of heterogeneity of a packing can be systematically varied via the algorithm input parameters ε_{fin} and α; (ii) the generated packings are isotropic as opposed to packings generated with sedimentation-based methods [45]; (iii) partial packing crystallization is avoided [46]; (iv) mono- or polydisperse packings can be generated in confined geometries with arbitrary cross-section [41]; and (v) the algorithm has a complexity of $O(n)$ [47], which enables the generation of packings containing millions of spheres at relatively low porosities ($\varepsilon \sim 0.4$) on one CPU core [42]. Compared with other popular computer algorithms [48,49] the JT algorithm is ideally suited to the study of dense, isotropic, random sphere packings in the porosity range most relevant for chromatography ($0.36 < \varepsilon < 0.40$).

In this study we represent varying degrees of microstructural disorder by four different types of packings. So-called *R*-packings originate from a random uniform initial distribution of particle centers in the simulation box. To generate *S*-packings, the simulation box was initially divided into n equal cubic cells and each particle

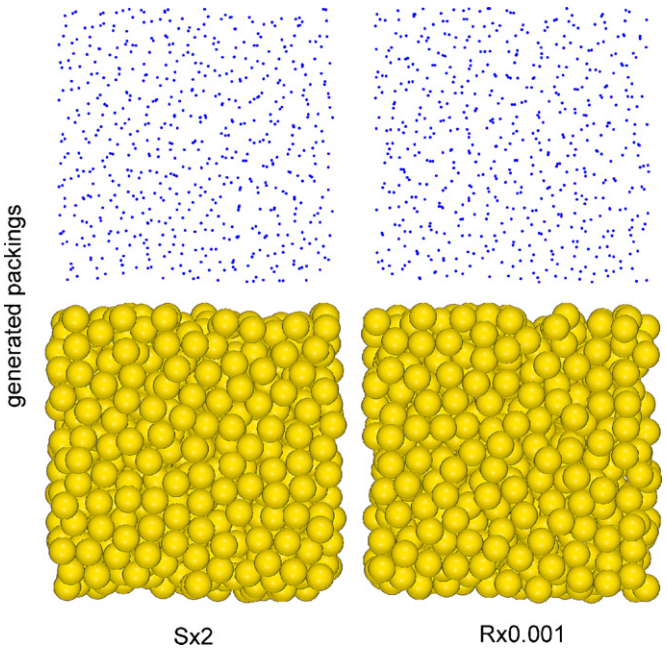

Fig. 1. Bulk (unconfined) random packings of monosized hard spheres at the random-loose packing limit ($\varepsilon = 0.46$), generated with the $S \times 2$ or $R \times 0.001$ packing protocols. Shown are the first three particle layers of the packings, as a front view (bottom) and as the projection of particle centers onto the front plane (top).

center was then placed in a random position into a cell. Both types of initial distributions result in a uniform random distribution of particle centers within the simulation box. *R*-packings were generated with $\alpha = 1$ (R) or $\alpha = 0.001$ ($R \times 0.001$), and *S*-packings with $\alpha = 1$ (S) or $\alpha = 2$ ($S \times 2$). With a small displacement value (cf. α in Eq. (2)) the particle centers tend to stay closer to their initial positions so that the final configuration reflects the randomness of the initial distribution of particle centers. A larger displacement value provides a more uniform distribution of particle centers in the final configuration. The four generated packing types therefore reflect a systematic decrease of heterogeneity (or disorder) in the sequence: $R \times 0.001 > R > S > S \times 2$.

Fig. 1 shows a front view onto three particle layers as well as a projection of the particle centers for the most ordered and the least ordered of the generated packings ($S \times 2$ and $R \times 0.001$, respectively). Even to the experienced eye, differences between the two packing microstructures are not discernible in Fig. 1. Therefore, we use two-dimensional views (disks instead of spheres) to illustrate the differences between the four different packing types and additionally replace the $S \times 2$ packing by a $S \times 6$ packing for a stronger effect (Fig. 2). For selected regions the microstructure of the final packings is compared with the respective initial particle center distributions in Fig. 2. The generated packings indeed reflect what was intended by their respective packing protocols: (i) *S*-packings are more homogeneous than *R*-packings, owing to the initial, ordered distribution of the disks, and (ii) initial nonuniformities are best balanced in the $S \times 6$ configuration and least balanced in the $R \times 0.001$ configuration.

Three-dimensional sphere packings of each type were generated at the following porosities: $\varepsilon = 0.366$, 0.38, 0.40, 0.42, 0.44, and 0.46. The border values ($\varepsilon = 0.366$ and 0.46) reflect the theoretical RCP and RLP limits reported by Song et al. [11]. They have shown that random hard-sphere packings in three dimensions cannot exceed a density limit of $\rho = 0.634$ (or $\varepsilon = 0.366$). Similarly, they predicted a theoretical limit for the lowest stable volume fraction occupied by a sphere packing of $\rho = 0.536$ ($\varepsilon = 0.464$).

For each packing protocol and porosity 10 individual packings were generated from 10 different initial positions of particle centers (seeds). We were not able to generate $S \times 2$ packings at the RCP limit ($\varepsilon = 0.366$). The total of all generated packings amounts to 230. Each packing was discretized with a relatively high spatial resolution of 60 nodes per d_p resulting in a space grid with dimensions of approximately $600 \times 600 \times 4300$ nodes. Each grid node was then assigned as either 'solid' or 'fluid' according to its position, i.e., within or outside the closest spherical particle.

3. Simulation of flow and dispersion

3.1. The lattice-Boltzmann method for fluid flow

The lattice-Boltzmann method (LBM) [50–53] was used for the simulation of low-Reynolds number flow of an incompressible fluid in the interparticle void space of the bulk packings. LBM has been

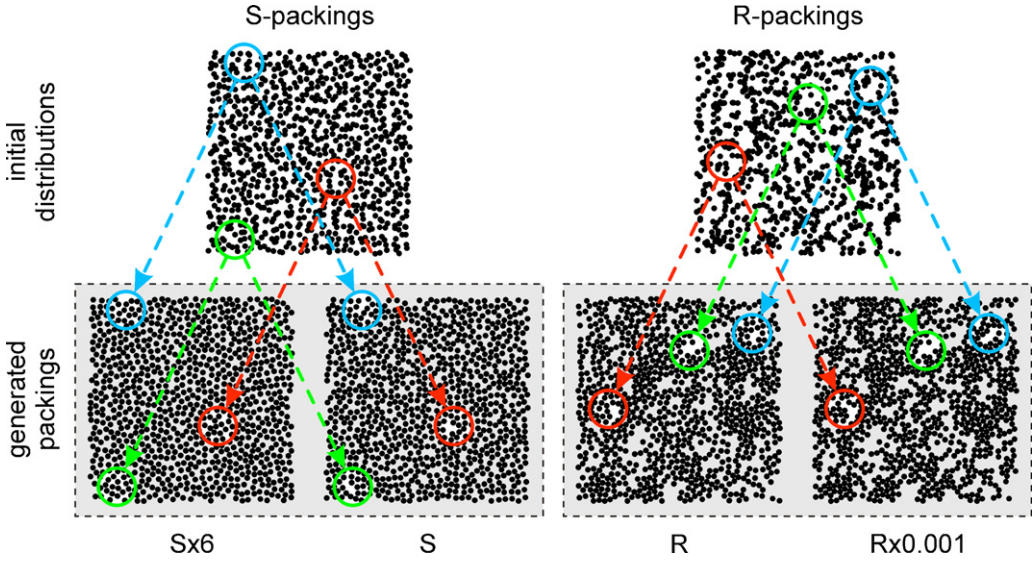

Fig. 2. Bulk (unconfined) random packings of monosized hard disks at $\varepsilon = 0.46$ generated with different packing protocols. Shown are the initial distributions of the disks for *S*- and *R*-configurations (top) and the generated two-dimensional packings ($S \times 6$, S, R, $R \times 0.001$; bottom). Circles around several regions help to compare the microstructure in the initial distributions with that of the final packings.

increasingly used to model pore-scale flow in systems with complex geometries like those found in porous media such as packed beds [23,27–34,36–43]. An advantage of this approach is its inherent parallelism, which allows easy parallelization of the developed numerical models for effective use on high-performance computing systems (supercomputers). We implemented the D3Q19-LBM, a three-dimensional 19-velocity lattice model [54]. Each site of this model demands 19×4 bytes of random access memory resulting in a final lattice size of $19 \times 4 \times 600 \times 600 \times 4300 \approx 110$ GB. At the solid–liquid interface, a bounce-back rule was applied [55]. It reproduces the 'no-slip' velocity boundary condition and Poiseuille flow profiles in straight microchannels [56] as well as between particles in a packed bed [57]. For each packing, the velocity field was first calculated at a low Reynolds number (~0.1), and the calculated velocity field was then linearly rescaled [33] to cover the whole velocity range used in the dispersion simulations.

All simulations were performed on IBM BlueGene/P systems installed at RZG (Rechenzentrum Garching, Germany) and FZJ (Forschungszentrum Jülich, Germany). A typical simulation of one velocity field required ~0.5 h on 2048 processor cores and around 420 GB of memory. After its simulation, the calculated velocity field was written into an output file with a size of ~17 GB.

3.2. Random-walk particle-tracking for tracer dispersion

Mass transfer in the bulk packings was simulated by a random-walk particle-tracking (RWPT) technique [58], where inert tracer particles are initially distributed randomly in the interparticle void space. During each time step δt, the displacement of each tracer particle is determined as the sum of convective and diffusive motions. Convective displacement of a tracer particle is calculated using a velocity vector from the nearest (to the tracer) lattice node, assuming that the fluid velocity is constant over the lattice voxel. Diffusive displacement in each spatial coordinate follows a Gaussian distribution with an average of zero and a variance of $(2D_m\delta t)^{1/2}$, where D_m is the diffusion coefficient. The time step δt was defined such that the average displacement did not exceed $\delta l/2$, where δl is the lattice spacing used to calculate the fluid flow velocity field.

Time-dependent longitudinal dispersion coefficients $D_L(t)$ were calculated from the tracer displacements as

$$D_L(t) = \frac{1}{2N}\frac{d}{dt}\sum_{i=1}^{N}(\Delta l_{z,i} - < \Delta l_z >)^2, \quad (3)$$

where N is the number of tracer particles ($N = 5 \times 10^5$), and $\Delta l_{z,i}$ and $\langle \Delta l_z \rangle$ are the Cartesian components of the longitudinal displacement of the ith tracer and the average longitudinal displacement of the tracer ensemble after time dt, respectively. Transverse dispersion coefficients $D_T(t)$, where needed (cf. Fig. 5A), were calculated similarly.

Hydrodynamic dispersion in the packings was simulated at reduced velocities (ν) or particle Péclet numbers (Pe), defined as $\nu \equiv Pe = u_{av}d_p/D_m$ (where u_{av} is the average mobile phase velocity through the packed bed), ranging from 0.5 to 750. The total simulation time of hydrodynamic dispersion for all generated packings was ~460 h on 2048 BlueGene/P processor cores. The program realization of all algorithms was implemented as parallel codes in C language using the Message Passing Interface (MPI) library [59,60].

4. Results and discussion

4.1. Statistical analysis of packed beds

A sensitive analysis tool for probing the local packing density and disorder in packed beds is the determination of Voronoï cells [61–64]. This method, initiated by Finney [65], has found increasing use for the characterization of the morphology of random sphere packings, including the study of, e.g., structural transitions upon compaction or the formation of coagulated colloids [19–22,66–74]. In particular, Schenker et al. [74] recently investigated and compared different methods to quantify and classify the disorder of particulate packings (in the context of stability and microstructure of coagulated colloids) based on (i) pore size distribution, (ii) density-fluctuation, and (iii) Voronoï volume distribution. Each of these methods provides a scalar measure, either via a parameter in a fit function or an integral, that correlates with the heterogeneity of the microstructure and thus allows to quantitatively capture the degree of heterogeneity of a granular material. They found that among the three methods, analysis of the Voronoï volume distributions reflected differences in the degree of microstructural heterogeneity most sensitively [74]. We therefore expect this method to be an excellent diagnostic tool for establishing a strong correlation between disorder and dispersion in packed beds.

A Voronoï cell is the generalization of a Wigner–Seitz cell for disordered structures. For a packing of monosized spheres it is the polyhedron that contains all points closer to a given sphere center than to any other [61–64] (as illustrated in Fig. 3A for a set of monosized disks; cf. the area encased by the bold red lines around disk center i). Voronoï tessellation partitions the whole space of a sphere packing into a set of non-overlapping Voronoï volumes V, which are inherently associated with the local packing density. The

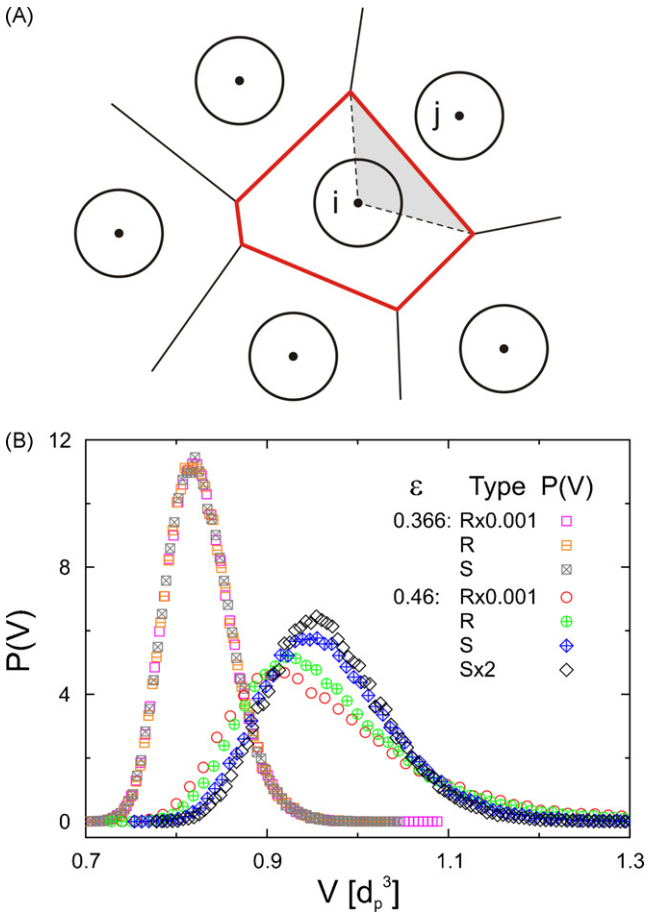

Fig. 3. (A) Voronoï cells in a two-dimensional array of disks. The Voronoï cell of disk i is encased by the bold red lines. The gray-shaded area indicates the contribution of disk j to the Voronoï area of disk i. (B) Voronoï volume distributions for the generated bulk sphere packings at the limiting porosities ($\varepsilon = 0.366$ and 0.46). (For interpretation of the references to color in this figure legend, the reader is referred to the web version of the article.)

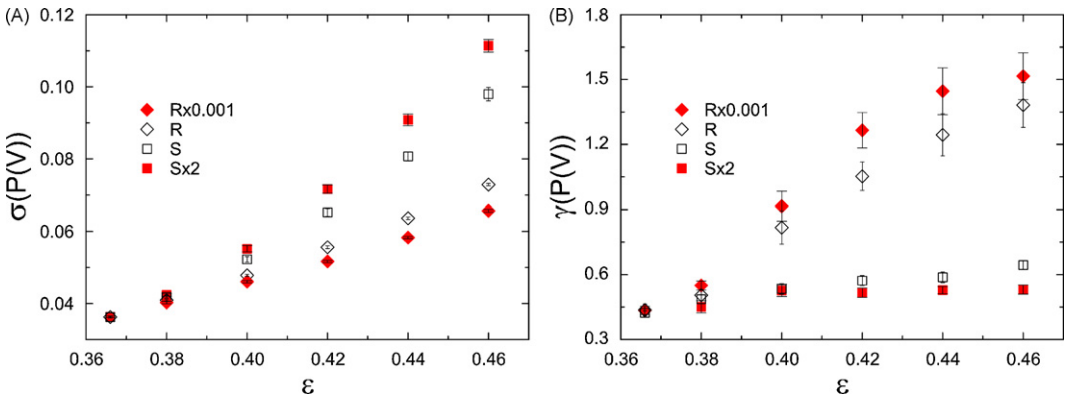

Fig. 4. Statistical analysis of the Voronoï volume distributions $P(V)$ for the bulk sphere packings (cf. Fig. 3B). (A) Standard deviation σ and (B) skewness γ as a function of packing protocol ($R \times 0.001$, R, S, $S \times 2$) and porosity ($0.366 \leq \varepsilon \leq 0.46$). Error bars indicate upper and lower bounds of 95% confidence intervals.

packing is represented quantitatively by the Voronoï volume distribution $P(V)$. The distribution function is defined such that $P(V)dV$ is the fraction of cells with a volume between V and $V+dV$. We used the Quickhull algorithm [75] to compute the volume V of the Voronoï cells.

Fig. 3B shows the Voronoï volume distributions for the generated packings at the limiting porosities, $\varepsilon = 0.366$ and 0.46. At the RCP limit ($\varepsilon = 0.366$), all Voronoï volume distributions are relatively narrow and symmetric, irrespective of the underlying packing protocol. They are nearly perfectly collapsed onto a single "universal" distribution. At the RLP limit ($\varepsilon = 0.46$) the distributions are shifted towards larger Voronoï volumes, as expected from the "dilution" of the packings at increasing porosity, and differences between the packing protocols emerge. Importantly, Voronoï volume distributions become wider and more asymmetric (skewed) with increasing microstructural heterogeneity in a packing. Thus, the $S \times 2$ packing has the narrowest and most symmetric Voronoï volume distribution at $\varepsilon = 0.46$, and the $R \times 0.001$ packing the broadest and most skewed, confirming the qualitative structural insight from Fig. 2.

Fig. 4 summarizes the statistical properties of the Voronoï volume distributions for the generated packings in terms of the standard deviation σ (Fig. 4A) and the skewness γ (Fig. 4B). These data quantify the effect of packing protocol and porosity as we move from the RCP ($\varepsilon = 0.366$) to the RLP limit ($\varepsilon = 0.46$) on the microstructural heterogeneity of a packing, already qualitatively discussed for Fig. 3B. At the RCP limit ($\varepsilon = 0.366$), the standard deviations $\sigma(P(V))$ are practically identical for all generated packings (Fig. 4A). With increasing porosity $\sigma(P(V))$ increases monotonically, and differences in $\sigma(P(V))$ between the packing types are visible from $\varepsilon = 0.40$. The skewness of the distribution $\gamma(P(V))$ is little affected by increasing porosity for the S-packings (Fig. 4B). Differentiation between R- and S-packings by $\gamma(P(V))$ starts already at $\varepsilon = 0.38$, and $\gamma(P(V))$ for the R-packings is rather sensitive towards increasing porosity. The strongest effect on the statistical parameters $\sigma(P(V))$ and $\gamma(P(V))$ in Fig. 4 comes from the principal difference between R- and S-packings, i.e., the random or ordered initial distribution of particle centers. Variation of the rate constant in the packing protocols (i.e., varying the distance over which particle centers can move away from their initial positions) affects the statistical parameters moderately and in the expected direction. Fig. 4 augments the qualitative picture of Fig. 2 by a thorough statistical analysis, demonstrating that the S-packings retain relatively narrow and symmetric Voronoï volume distributions even at increasing porosity (as opposed to the R-packings), and that the four generated packing types are indeed characterized by a systematic decrease of disorder in the sequence: $R \times 0.001 > R > S > S \times 2$.

The Voronoï volume distributions in Fig. 4 describe the degree of deviation of a given packing type from a perfectly crystalline packing. All spheres in a crystal are associated with the same Voronoï volume, so that the Voronoï volume distribution is a delta function. For the studied random bulk packings the Voronoï volume distributions become wider and more asymmetric as we move from the RCP ($\varepsilon = 0.366$) to the RLP limit ($\varepsilon = 0.46$). Their standard deviation and skewness can then be used to express and quantify the heterogeneity of a packing (Fig. 4), analogous to the familiar analysis of separation efficiency from the width and skewness of peaks in a chromatogram.

For completeness we mention that Aste and Di Matteo [73] deduced by statistical mechanics that the Voronoï volume distributions for monodisperse random sphere packings follow a so-called two-parameter 'k-Gamma' function, in which k, the shape parameter of the curve, depends sensitively on the packing microstructure. Furthermore, we also conducted a Delaunay tessellation [21,64] of the generated packings, but found a stronger correlation between dispersion and disorder with the statistical moments of the Voronoï volume distributions.

Our findings (Fig. 4) agree with those of closely related investigations [66,70,73], where the dilution of particle packings was always accompanied by broadening and increasing asymmetry of the Voronoï volume distributions. Packings at the RCP limit show merely statistical variations in standard deviation and skewness of their Voronoi volume distributions (Figs. 3 and 4), because the constraints of the RCP limit on the placement of particles allow for so little variation in packing microstructure that the different protocols used in this study will nonetheless yield very similar packings [8,11,20–22]. At the other extreme of stable packings, the RLP limit, the spheres experience more freedom of placement and differences between the packing types are clearly reflected in their Voronoï volume distributions. This behavior can be visualized with a formal analogy between the statistical mechanics of granular jammed matter and classical statistical mechanics: the microcanonical ensemble, defined by all microstates with fixed energy, is replaced by the ensemble of all jammed microstates with fixed volume [7]. Within this notion, the RCP limit of spheres can be interpreted as the ground state of the ensemble of jammed matter for a given friction (see, e.g., the volume landscape of jammed matter, Fig. 2 in [11]).

4.2. Transient and asymptotic dispersion

We simulated eddy dispersion in the generated packings to correlate the quantified microstructural disorder with the transport properties most relevant to chromatography. The longitudinal dispersion coefficient D_L usually discussed in the engineering liter-

ature [76] is related to chromatographic plate height H by [77]

$$D_L = \frac{u_{av}H}{2} = \frac{\nu D_m h}{2}, \quad (4)$$

where $h = H/d_p$ denotes reduced plate height and ν is the reduced velocity introduced earlier. The flow pattern of a fluid depends critically on the morphology of the pore space available for the flow, so that the inherent structural heterogeneities of the packed beds investigated in this work determine time and length scales that characterize velocity fluctuations in the mobile phase [33,42,77–82].

By applying the random–walk relationship to a model of eddy dispersion incorporating the coupling between transverse diffusion and spatial velocity fluctuations, Giddings [77] developed a plate height equation by analogy to parallel conductors. The comprehensive equation for $h = f(\nu)$ is

$$h = \frac{b}{\nu} + \sum_{i=1}^{4} \frac{2\lambda_i}{1 + (2\lambda_i/\omega_i)\,\nu^{-1}} + c\nu. \quad (5)$$

The first term on the right-hand side of Eq. (5), b/ν, accounts for the effect of longitudinal molecular diffusion in the packed bed driven by the concentration gradient along the zone profile [82]. The second term in Eq. (5) describes eddy dispersion as the sum of four contributions used to model the erratic mass transfer by flow and diffusion in the interparticle pore space of a packing on different length scales (transchannel, short-range interchannel, long-range interchannel, and transcolumn), where λ_i and ω_i are universal structural parameters characteristic of each contribution, and the ratio $\nu_{1/2} = 2\lambda_i/\omega_i$ is a reduced transition velocity for each type of velocity disparity. It is the velocity at which the corresponding plate height term reaches half of its limiting value and thereafter begins to flatten noticeably [83]. The last term in Eq. (5), $c\nu$, accounts for the mass transfer kinetics from the bulk solution into and across the particles [84].

To our knowledge the challenge of resolving systematically, either by experiment or simulation, the different structural parameters characteristic of each contribution to the eddy dispersion term of the comprehensive Giddings equation (Eq. (5)) has never been undertaken. Past investigations in this direction [33,85–87] are all in favor of Giddings' coupling theory of eddy dispersion, but the analysis remained limited to the "simple" Giddings equation, i.e., Eq. (5) with $i = 1$.

Recent progress in our understanding of the time and length scales as well as the magnitude of individual contributions to eddy dispersion in chromatographic beds stems from a high-resolution numerical analysis of flow and mass transport in computer-generated bulk packings of spherical particles and complementary confined cylindrical packings with a cylinder-to-particle diameter ratio of 20 [42]. The transient behavior of longitudinal and transverse dispersion was analyzed and correlated with the spatial scales of heterogeneity in the bulk and confined packings. It was found that the total effect of eddy dispersion on the plate height curves can be approximated in the practical range of chromatographic operational velocities by a composite expression in which only the short-range interchannel contribution retains its coupling characteristics, whereas transchannel and transcolumn contributions appear as simple velocity-proportional terms.

In the previous [42] as well as in the present work, the choice of packing protocols, porosities, and operating conditions in our numerical analysis approach facilitates the focus on eddy dispersion and its precise dependence on the morphology of the packed beds. The selection of perfectly monosized, spherical particles allows the strict operation with reduced parameters ($h = H/d_p$ and $\nu = u_{av}d_p/D_m$) without influence from the particle size distribution and particle shape. The use of nonporous support particles and inert conditions (unretained tracer particles) eliminates mass transfer resistance contributions ($c = 0$ in Eq. (5)) [86,87]. Although it has sometimes been claimed that even with solid particles and unretained tracers a remaining c-term in Eq. (5) is needed to account for pore-scale Taylor dispersion, we like to emphasize that this contribution is already contained in the eddy dispersion term of Eq. (5) as the transchannel contribution. In deriving Eq. (5) under most general conditions, Giddings has pooled all mass transfer resistances in the mobile phase (as distinguished from diffusion and adsorption/desorption in the stationary phase) into the coupling expression of Eq. (5) (cf. derivation of Eq. (2.11–1) on p. 62 in [77] and the transition to Eq. (2.11–2)).

For the packings and conditions considered in our analysis, the coefficient accounting for the contribution of longitudinal diffusion to the reduced plate height in Eq. (5) is $b = 2\gamma$, where γ is the obstruction factor often used in chromatography [77,88]. It is the inverse of the tortuosity factor (τ) of the interconnected pore space usually used in the engineering literature [76] and is defined as

$$\gamma = \lim_{t\to\infty} \frac{D(t)}{D_m} = \frac{1}{\tau} = \frac{D_{eff}}{D_m}, \quad (6)$$

where D_{eff} is the effective diffusion coefficient in the sphere packing, i.e., its asymptotic value observed in the long-time limit for $\nu = 0$.

The packed beds in this work mimic infinitely wide, unconfined random sphere packings, suitable for the study of eddy dispersion as related to bulk microstructural properties without the complex influence of wall effects [31,34,37–39,42,89–91]. To quantify the time and length scales behind the velocity heterogeneities from different packing microstructures, we analyze the development of longitudinal dispersion coefficients $D_L(t)$. Monitoring the transient behavior of the dispersion process towards asymptotic values allows to distinguish between individual contributions to eddy dispersion, especially with regard to the upper limit of the involved time and length scales. This helps to condense, where physically meaningful, the number of scales of velocity disparity in a packing proposed by Giddings [77]. In the investigated bulk packings, we expect only the transchannel and a short-range interchannel effect to contribute to eddy dispersion.

Fig. 5A shows the development of normalized longitudinal dispersion coefficients $D_L(t)/D_m$ at $\nu = 50$ for the $R \times 0.001$ packings at three porosities ($\varepsilon = 0.366$, 0.42, and 0.46). Elapsed time here has been normalized through the transverse dispersive time $\tau_D = 2D_T t/{d_p}^2$. The dispersive time unit $2D_T/{d_p}^2$ corresponds to the time span after which tracer particles are dispersed laterally by one sphere diameter. The use of the transverse dispersive time scale is important here, because neither pure diffusion nor pure convection determines the lateral equilibration between different velocities, which instead would have resulted in a diffusive ($\tau_D = 2D_m t/{d_p}^2$) or a convective ($\tau_C = u_{av}t/d_p$) time scale. The use of $D_T(\nu)$ in the dimensionless dispersive time scale τ_D (Fig. 5A) reflects the actual combination of flow and diffusion, which is also the essence of Giddings' coupling theory [77].

All generated packings, irrespective of their packing protocol, demonstrate asymptotic dispersion for $\tau_D < 2$ throughout the whole porosity range ($\varepsilon = 0.366$–0.46), as shown exemplarily for the $R \times 0.001$ packings in Fig. 5A. However, as the porosity decreases from $\varepsilon = 0.46$ to $\varepsilon = 0.366$, the transient dispersion domain shrinks, i.e., asymptotic dispersion is reached faster (cf. Fig. 5A). This is readily explained by our previous analysis (Fig. 4) to originate from the accompanying decrease of local disorder in the packing microstructures. The time scale of $\tau_D = 2D_T t/{d_p}^2 \approx 2$ translates to a characteristic average transverse dispersion length in the bulk packings $\langle \ell_T \rangle$ of

$$\langle \ell_T \rangle = \sqrt{2D_T(\nu)t} \approx \sqrt{2}d_p. \quad (7)$$

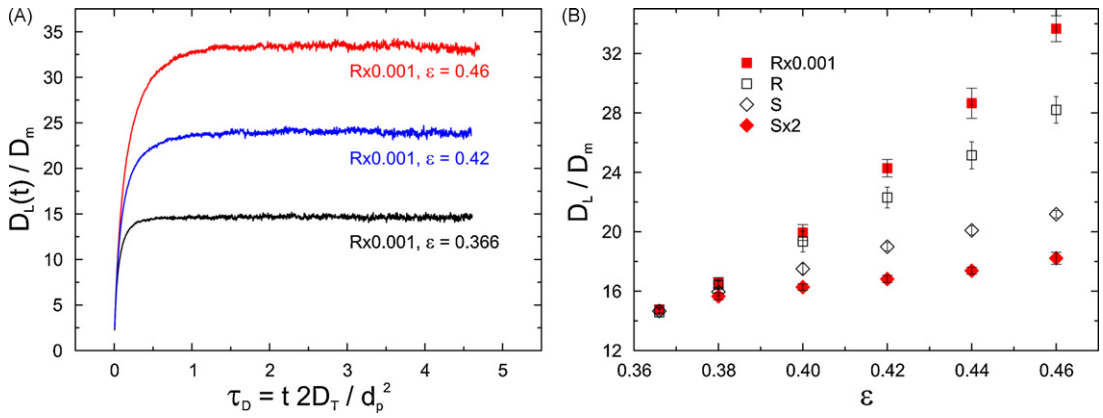

Fig. 5. (A) Time evolution of normalized longitudinal dispersion coefficients $D_L(t)/D_m$ at $\nu = u_{av}d_p/D_m = 50$ for $R \times 0.001$ packings at porosities of $\varepsilon = 0.366$, 0.42, and 0.46. (B) Normalized asymptotic dispersion coefficients D_L/D_m at $\nu = 50$ for all generated packings as a function of packing protocol and porosity. Error bars indicate upper and lower bounds of 95% confidence intervals.

Thus, dispersion in the bulk packings is asymptotic after a distance of about $1.4d_p$ (or less, depending on the packing protocol and porosity) has been sampled laterally by the tracer particles.

The analysis of longitudinal dispersion confirms our surmise that a short-range disorder is responsible for the upper limit in the time and length scales of eddy dispersion in the bulk packings. Whereas transchannel equilibration (length scale $\ll d_p$) is required in any packed bed, ordered or random, the short-range heterogeneity observed here is associated with the disorder in a random sphere packing as compared with a crystalline packing. Our characterization of a short-scale heterogeneity on the order of $1–1.5d_p$ (Fig. 5A, Eq. (7)) compares favorably with the distance of $\sim 1.25d_p$ required for exchanging molecules between the involved velocity extremes estimated by Giddings (p. 45 in [77]).

Fig. 5B contains the asymptotic longitudinal dispersion coefficients (D_L/D_m) for all generated packings at $\nu = 50$. The data are immediately reminiscent of those in Fig. 4, i.e., the dispersion coefficients and (particularly) the standard deviations of the Voronoï volume distributions (Fig. 4A) show highly similar dependencies on packing protocol and porosity. From this we conclude that the width of the Voronoï volume distribution of a packing is a sensitive measure for its disorder that closely correlates with the dispersion in the packing.

To summarize, our analysis of transient dispersion in the bulk sphere packings reveals a short-range interchannel contribution on the single-particle scale ($1–1.5d_p$) in addition to the transchannel contribution, which naturally exists in any packed bed on the scale of an individual channel between the particles ($\ll d_p$). Thus, all packings investigated in this work can be characterized as relatively homogeneous, even though they were generated to reflect individual local disorder (Figs. 2-4). Structural and flow heterogeneities beyond the documented short-scale (cf. Fig. 5A, Eq. (7)) cannot be resolved.

This knowledge is extremely helpful in analyzing the dependence of reduced plate heights on the reduced velocity, $h = f(\nu)$, by the comprehensive Giddings equation (Eq. (5)), as it allows to reduce the number of eddy dispersion contributions to the transchannel and the short-range interchannel effect (Eq. (5) with $i = 2$). Thus, we use the following form of Eq. (5) to fit the dependence of reduced plate heights (calculated from the asymptotic values of D_L/D_m – see Fig. 5A – via Eq. (4)) on the reduced velocity for the generated bulk packings (cf. Eq. (2.11–6) on p. 63 in [77])

$$h = \frac{2\gamma}{\nu} + \underbrace{\frac{2\lambda_1}{1 + (2\lambda_1/\omega_1)\nu^{-1}}}_{\text{transchannel}} + \underbrace{\frac{2\lambda_2}{1 + (2\lambda_2/\omega_2)\nu^{-1}}}_{\text{short-range interchannel}}, \quad (8)$$

where indices 1 and 2 refer to the transchannel and the short-range interchannel contribution to eddy dispersion, respectively. As explained above, the use of nonporous support particles and unretained tracer particles gives $c = 0$ in Eq. (5).

The $h–\nu$ curves for the four different types of bulk packings are presented in Fig. 6. Each curve contains 29 values for h over the range of $0.5 \le \nu \le 750$, with each h value representing the average from 10 individual packings of a given type and porosity. For packings at the limiting porosities ($\varepsilon = 0.366$ and $\varepsilon = 0.46$) the best fits of the $h–\nu$ data to the condensed Giddings equation for bulk packings (Eq. (8)) are also shown. Eq. (8) fits excellently the simulated plate height data over the whole range of reduced velocities ($R^2 > 0.999$). The shift of the plate height curves as the porosity increases from $\varepsilon = 0.366$ to $\varepsilon = 0.46$ reveals the degree to which the porosity increases the disorder and therefore the dispersion in a particular packing type. The plate height curves for the most ordered packing type, the $S \times 2$ packings, are hardly affected by a porosity increase, whereas those for the least ordered packing type, the $R \times 0.001$ packings, span a relatively large range. For example, the curve minimum for the $R \times 0.001$ packings shifts from the universal (to all packing types) minimum at the RCP limit at $h_{min} = 0.5$ and $\nu_{min} = 10$ to $h_{min} = 1$ and $\nu_{min} = 5$ at the RLP limit. The disparate sensitivities of the various packing types towards increased porosity underline the importance of the packing method for dispersion in (and ultimately the separation efficiency of) a packed bed.

The parameters for the transchannel (λ_1, ω_1) and the short-range interchannel contribution (λ_2, ω_2) obtained from the fitting of the comprehensive dataset of Fig. 6 are summarized in Fig. 7. Values for the obstruction factor $\gamma = D_{eff}/D_m$ (Eq. (6)) were obtained independently by monitoring the long-time (tortuosity) limit of the diffusion coefficient D_{eff} in the generated bulk packings, analogous to $D_L(t)/D_m$ in Fig. 5A, but for $\nu = 0$. In this way, the contribution of longitudinal diffusion to the dispersion (first term on the right-hand side of Eq. (8)) can be determined separately and with high precision [42]. The values of γ range from ~ 0.65 (for all packings at the RCP limit) to ~ 0.71 (for the $S \times 2$ packings at the RLP limit). The received γ value for each packing was then fixed during fitting of the $h–\nu$ data in Fig. 6 to Eq. (8). The values of Fig. 7 should now be compared with the estimates of Giddings [77], who did not include their dependence on packing method or porosity, but was certainly well aware at his time that both factors influence the final packing microstructure. Giddings estimated values of $\lambda_1 \sim 0.5$, $\omega_1 \sim 0.01$, $\lambda_2 \sim 0.5$, and $\omega_2 \sim 0.5$ [77]. We recognize that our values in Fig. 7 genuinely reflect his estimates made more than forty years ago. Concerning the remaining differences in the "universal" structural parameters (λ_i and ω_i) it should be noted that the exact geometrical and topological differences between the

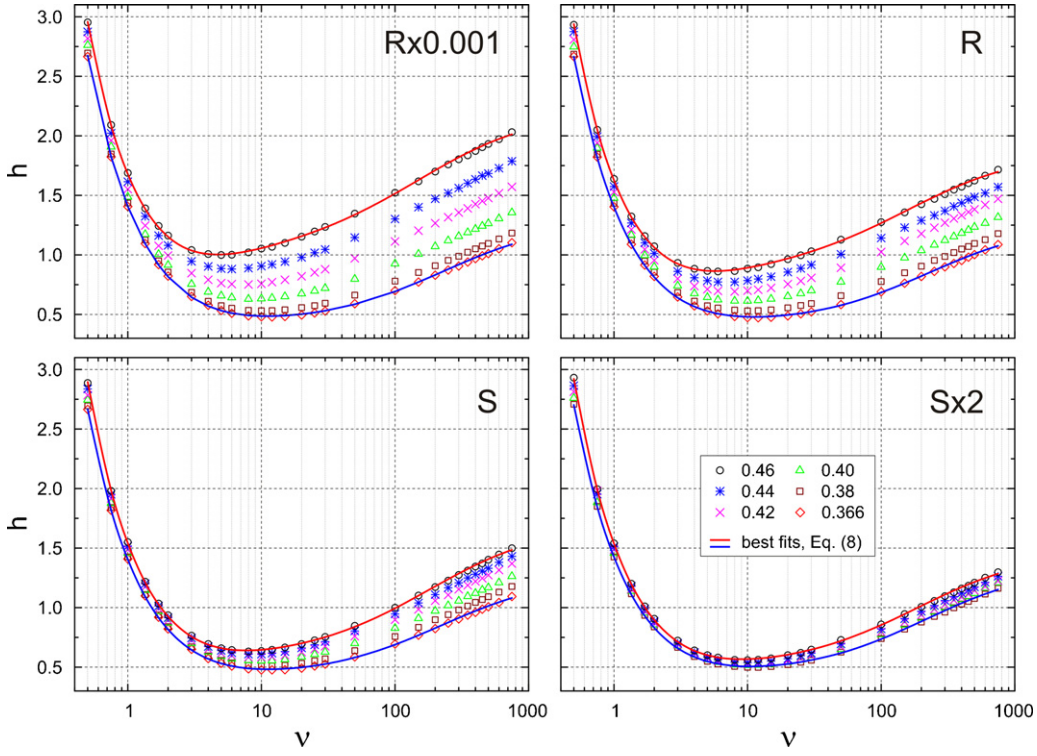

Fig. 6. Dependence of the reduced plate height $h = H/d_p$ on the reduced velocity $\nu = u_{av}d_p/D_m$ ($0.5 \le \nu \le 750$) and the porosity ($0.366 \le \varepsilon \le 0.46$) for the four different types of bulk packings ($R \times 0.001$, R, S, $S \times 2$). Each value of h represents the average from 10 generated packings. Solid lines are the best fits of the data at $\varepsilon = 0.366$ and 0.46 to Eq. (8).

packed beds analyzed by Giddings and those studied in this work (and particularly those encountered in chromatographic practice) are hardly known with sufficient accuracy to allow for meaningful quantitative distinctions. But exactly this missing link is provided in the current work by the complementary statistical analysis of the packed beds (Figs. 3 and 4), which quantifies their disorder.

Comparison of Fig. 7 with Fig. 4 now rounds off our structure–transport analysis from packing generation via statistical

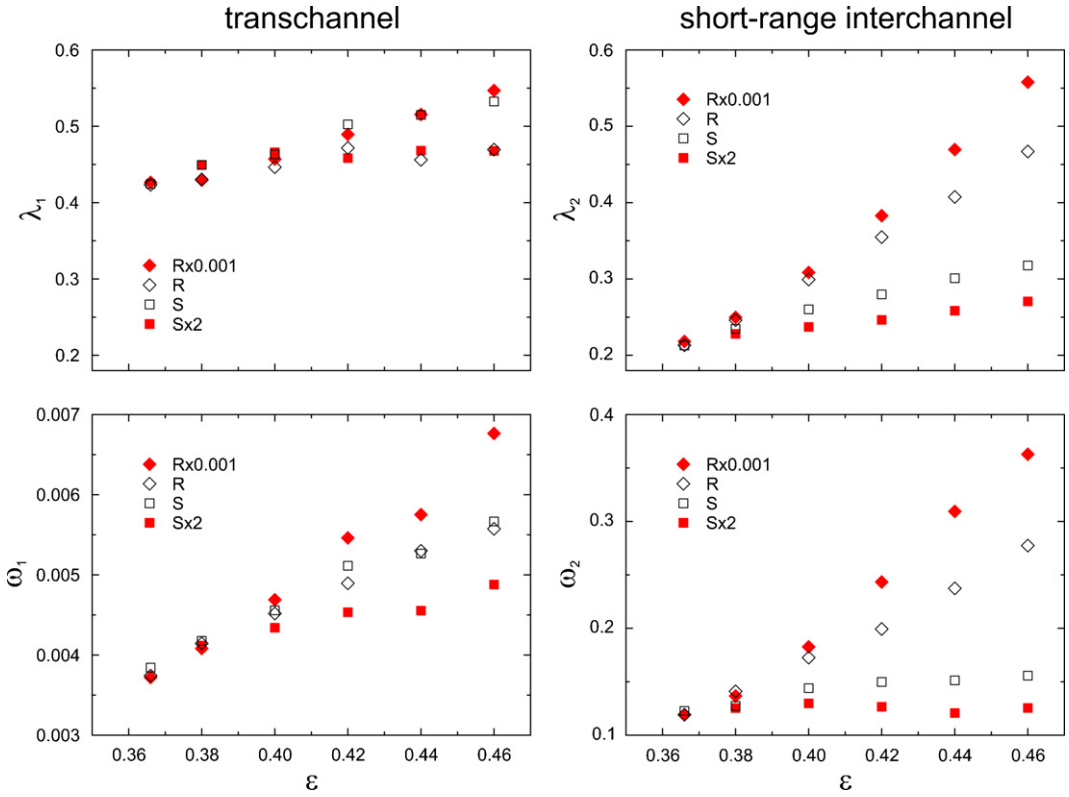

Fig. 7. Dependence of the parameters for the transchannel contribution (λ_1 and ω_1; left column) and the short-range interchannel contribution (λ_2 and ω_2; right column) on packing protocol and porosity. Values were obtained from the best fits of the comprehensive dataset of Fig. 6 to the condensed Giddings equation for bulk packings, Eq. (8).

mechanics to hydrodynamics and chromatography. We particularly note the strong correlation between the dependencies on generation protocol and porosity of the short-range interchannel effect (λ_2, ω_2) in Fig. 7 and both the standard deviation (σ) and skewness (γ) of the Voronoï volume distributions reported in Fig. 4. Thus, both statistical measures of the Voronoï volume distributions (σ, γ) are excellent, quantitative descriptors of the short-range disorder in the generated packings. This confirms that the deviation of the Voronoï volume distributions in Fig. 3 from the delta function characterizing a crystalline packing describes the origin of short-range disorder, and the statistical measures in Fig. 4 therefore represent particle packings with an individual, local randomness in their microstructure.

In addition to the strong correlation between our statistical measures (Fig. 4) and the parameters λ_2 and ω_2 characterizing the short-range interchannel effect (right column in Fig. 7), we also note a weaker correlation of the statistical measures with the parameter ω_1 for the transchannel effect in Fig. 7. This is expected, because the value of ω_1 depends on the lateral dimensions of the interparticle pores in a packed bed (pp. 43–44 in [77]), thus, also on the porosity and individual generation of a packing. Further, we observe little or no correlation between the statistical measures in Fig. 4 and the parameter λ_1 for the transchannel effect (Fig. 7). The values of λ_1 scatter around ~0.48 (close to Giddings' value of 0.5 [77]). In this respect, the velocity inequality between the center and the wall regions of a pore may be envisioned as lasting along the length of a single particle, after which the flow will split up into several subsequent pores (pp. 49–50 in [77]). Therefore, the value of λ_1 is little or not affected by the local disorder encountered in this work. To summarize, the analysis of short-range disorder based on the Voronoï volume distributions (Fig. 4) shows the expected strong correlation with the short-range interchannel contribution to eddy dispersion in Eq. (8), whereas the transchannel contribution is relatively little affected.

Finally, by examining the above-determined structural parameters (λ_i, ω_i) we identify the short-range interchannel effect as being responsible for a convex upward bending of the eddy dispersion curve at low velocities. The transchannel effect causes the eddy dispersion curve (and overall plate height data) to taper off at high velocities. This is easily understood by calculating the transition velocities $\nu_{1/2} = 2\lambda_i/\omega_i$ for each contribution to eddy dispersion at which the plate height term reaches half of its limiting value and thereafter begins to flatten noticeably [83]. Where $\nu_{1/2}$ is large (~200 for the transchannel effect) the contribution to the reduced plate height continues to increase with velocity over a significant range of the plots in Fig. 6, the same as for an ordinary kinetics or mass transfer velocity-proportional term, whereas the plate height contribution of the short-range interchannel effect ($\nu_{1/2} \sim 3$) reaches its plateau at relatively low velocities.

The high transition velocities of the transchannel contribution indicate that in a practical range of chromatographic operation, i.e., at reduced velocities of about $5 \leq \nu \leq 20$, this effect reduces to a simple mass transfer velocity-proportional term, i.e., for $(2\lambda_i/\omega_i) \gg \nu$, the transchannel contribution can be expressed by $\omega_1 \nu$. Only the short-range interchannel contribution retains its coupling characteristics. The total effect of the component plate height curves to eddy dispersion can then be written in the form

$$h_{\text{eddy}} = \omega_1 \nu + \frac{2\lambda_2}{1 + (2\lambda_2/\omega_2)\nu^{-1}}. \quad (9)$$

This result agrees very well with the scale analysis for bulk packings in our previous work [42]. The relatively low impact of coupling between diffusive and flow mechanisms of eddy dispersion in this limited range of velocities ($5 \leq \nu \leq 20$) also explains why the van Deemter equation [92] remains an accurate description of plate height data in that case, particularly with porous particles, when the mass transfer terms associated with the stationary phase are added [85,93].

5. Conclusions

Statistical analysis of packed beds by the standard deviation and skewness of the Voronoï volume distributions (Figs. 3B and 4) provides quantitative scalar measures for local disorder in packing microstructure that correlate strongly with the resulting eddy dispersion (Figs. 5B and 6). Therefore, the presented approach defines a straight route to quantitative structure–transport relationships, replacing popularized views based on heuristics [94]. Transport phenomena relevant to chromatography can be analyzed in detail by direct numerical simulations (realized on an efficient high-performance computing platform) and correlated, e.g., with the generalized Giddings equation (Figs. 6 and 7). Complementary analysis of the transient dispersion domain allows to identify the spatial scales of disorder in the packings, which helps to condense the number of scales of velocity disparity in a packing proposed by Giddings [77]. In the investigated bulk packings, we identified only the transchannel and a short-range interchannel effect to contribute to eddy dispersion (Fig. 5A). This result is in excellent agreement with our statistical analysis based on the Voronoï volume distributions, which revealed a packing porosity and protocol-dependent short-range disorder, in a strong correlation with the short-range interchannel contribution to eddy dispersion (Figs. 4 and 7).

Future refinements in packing generation will focus on the physicochemical properties of the particles like surface roughness and chemical modification, as well as on nonuniform particle shape and size distributions. In experimental packings these effects are inherently included. The microstructure of experimental packings (e.g., in a chromatographic column) – though not as easily accessible (and at high precision) as those of simulated packings – may be analyzed by suitable techniques such as nuclear magnetic resonance imaging and confocal laser scanning microscopy. Comparison of experimental and simulated microstructures will help to differentiate systematically between packing algorithms and protocols used in simulations and experimental studies. This could also provide a new approach to column packing and consolidation, which traditionally are largely treated phenomenologically and considered an art rather than a science.

Acknowledgement

This work was supported by the Deutsche Forschungsgemeinschaft DFG (Bonn, Germany) under grant TA 268/4-1. Computational resources on IBM BlueGene/P platforms were provided by "Genius" at RZG (Rechenzentrum Garching, Germany) and "Jugene" at FZJ (Forschungszentrum Jülich, Germany). We thank the DEISA Consortium (www.deisa.eu), co-funded through the EU FP6 project RI-031513 and the FP7 project RI-222919, for support within the DEISA Extreme Computing Initiative.

References

[1] S. Torquato, Random Heterogeneous Materials, Springer, New York, 2002.
[2] J.D. Bernal, Nature 183 (1959) 141.
[3] J.D. Bernal, J. Mason, Nature 188 (1960) 910.
[4] J.D. Bernal, Proc. R. Soc. Lond. A 280 (1964) 299.
[5] T. Aste, D. Weaire, The Pursuit of Perfect Packing, Institute of Physics Publishing, Bristol, 2000.
[6] A. Coniglio, A. Fiero, H.J. Herrmann, M. Nicodemi (Eds.), Unifying Concepts in Granular Media and Glasses, Elsevier, Amsterdam, 2004.
[7] S.F. Edwards, R.B.S. Oakeshott, Physica A 157 (1989) 1080.
[8] S. Torquato, T.M. Truskett, P.G. Debenedetti, Phys. Rev. Lett. 84 (2000) 2064.
[9] S. Torquato, F.H. Stillinger, J. Phys. Chem. B 105 (2001) 11849.
[10] K. Bagi, Granular Matter 9 (2007) 109.
[11] C. Song, P. Wang, H.A. Makse, Nature 453 (2008) 629.

[12] C. Briscoe, C. Song, P. Wang, H.A. Makse, Phys. Rev. Lett. 101 (2008) 188001.
[13] N.Ch. Karayiannis, K. Foteinopoulou, M. Laso, Phys. Rev. E 80 (2009) 011307.
[14] G. Guiochon, J. Chromatogr. A 1126 (2006) 6.
[15] K.K. Unger, R. Skudas, M.M. Schulte, J. Chromatogr. A 1184 (2008) 393.
[16] B.G. Yew, J. Ureta, R.A. Shalliker, E.C. Drumm, G. Guiochon, AIChE J. 49 (2003) 642.
[17] H.P. Zhu, Z.Y. Zhou, R.Y. Yang, A.B. Yu, Chem. Eng. Sci. 62 (2007) 3378.
[18] H.P. Zhu, Z.Y. Zhou, R.Y. Yang, A.B. Yu, Chem. Eng. Sci. 63 (2008) 5728.
[19] T. Aste, M. Saadatfar, T.J. Senden, Phys. Rev. E 71 (2005) 061302.
[20] R.D. Kamien, A.J. Liu, Phys. Rev. Lett. 99 (2007) 155501.
[21] A.V. Anikeenko, N.N. Medvedev, T. Aste, Phys. Rev. E 77 (2008) 031101.
[22] T. Aste, T. Di Matteo, Eur. Phys. J. B 64 (2008) 511.
[23] C.P. Lowe, D. Frenkel, Phys. Rev. Lett. 77 (1996) 4552.
[24] D. Coelho, J.-F. Thovert, P.M. Adler, Phys. Rev. E 55 (1997) 1959.
[25] K.E. Thompson, H.S. Fogler, AIChE J. 43 (1997) 1377.
[26] S. Stapf, K.J. Packer, R.G. Graham, J.-F. Thovert, P.M. Adler, Phys. Rev. E 58 (1998) 6206.
[27] B. Manz, L.F. Gladden, P.B. Warren, AIChE J. 45 (1999) 1845.
[28] R.S. Maier, D.M. Kroll, R.S. Bernard, S.E. Howington, J.F. Peters, H.T. Davis, Phys. Fluids 12 (2000) 2065.
[29] M.D. Mantle, A.J. Sederman, L.F. Gladden, Chem. Eng. Sci. 56 (2001) 523.
[30] R.J. Hill, D.L. Koch, A.J.C. Ladd, J. Fluid Mech. 448 (2001) 243.
[31] R.S. Maier, D.M. Kroll, R.S. Bernard, S.E. Howington, J.F. Peters, H.T. Davis, Philos. Trans. R. Soc. Lond. A 360 (2002) 497.
[32] D. Kandhai, D. Hlushkou, A.G. Hoekstra, P.M.A. Sloot, H. Van As, U. Tallarek, Phys. Rev. Lett. 88 (2002) 234501.
[33] M.R. Schure, R.S. Maier, D.M. Kroll, H.T. Davis, Anal. Chem. 74 (2002) 6006.
[34] R.S. Maier, D.M. Kroll, R.S. Bernard, S.E. Howington, J.F. Peters, H.T. Davis, Phys. Fluids 15 (2003) 3795.
[35] P. Magnico, Chem. Eng. Sci. 58 (2003) 5005.
[36] D. Hlushkou, A. Seidel-Morgenstern, U. Tallarek, Langmuir 21 (2005) 6097.
[37] H. Freund, J. Bauer, T. Zeiser, G. Emig, Ind. Eng. Chem. Res. 44 (2005) 6423.
[38] M.R. Schure, R.S. Maier, J. Chromatogr. A 1126 (2006) 58.
[39] R.S. Maier, D.M. Kroll, H.T. Davis, AIChE J. 53 (2007) 527.
[40] R.S. Maier, M.R. Schure, J.P. Gage, J.D. Seymour, Water Resour. Res. 44 (2008) W06S03.
[41] S. Khirevich, A. Höltzel, S. Ehlert, A. Seidel-Morgenstern, U. Tallarek, Anal. Chem. 81 (2009) 4937.
[42] S. Khirevich, A. Höltzel, A. Seidel-Morgenstern, U. Tallarek, Anal. Chem. 81 (2009) 7057.
[43] R.S. Maier, R.S. Bernard, J. Comput. Phys. 229 (2010) 233.
[44] W.S. Jodrey, E.M. Tory, Phys. Rev. A 32 (1985) 2347.
[45] E.M. Tory, N.A. Cochrane, S.R. Waddell, Nature 220 (1968) 1023.
[46] A.Z. Zinchenko, J. Comput. Phys. 114 (1994) 298.
[47] M. Bargieł, J. Mościński, Comp. Phys. Commun. 64 (1991) 183.
[48] J. Tobochnik, P.M. Chapin, J. Chem. Phys. 88 (1988) 5824.
[49] W.M. Visscher, M. Bolsterli, Nature 239 (1972) 504.
[50] S. Chen, G.D. Doolen, Annu. Rev. Fluid Mech. 30 (1998) 329.
[51] S. Succi, The Lattice Boltzmann Equation: For Fluid Dynamics and Beyond, Oxford University Press, New York, 2001.
[52] D. Raabe, Modell. Simul. Mater. Sci. Eng. 12 (2004) R13.
[53] S. Ubertini, G. Bella, S.A. Orszag, S. Succi (Eds.), Lectures on Lattice Boltzmann Methods for Complex Fluid Flows, Consorzio S.C.I.R.E., Science4 Press, 2009.
[54] Y.H. Qian, D. d'Humières, P. Lallemand, Europhys. Lett. 17 (1992) 479.
[55] M.A. Gallivan, D.R. Noble, J.G. Georgiadis, R.O. Buckuis, Int. J. Numer. Methods Fluids 25 (1997) 249.
[56] D. Hlushkou, D. Kandhai, U. Tallarek, Int. J. Numer. Methods Fluids 46 (2004) 507.
[57] D. Hlushkou, S. Khirevich, V. Apanasovich, A. Seidel-Morgenstern, U. Tallarek, Anal. Chem. 79 (2007) 113.
[58] F. Delay, P. Ackerer, C. Danquigny, Vadose Zone J. 4 (2005) 360.
[59] W. Gropp, E. Lusk, A. Skjellum, Using MPI: Portable Parallel Programming with the Message-Passing Interface, MIT Press, Cambridge, MA, 1999.
[60] Message Passing Interface, http://www-unix.mcs.anl.gov/mpi (03.2010).
[61] G. Voronoï, J. Reine Angew. Math. 133 (1908) 97.
[62] G. Voronoï, J. Reine Angew. Math. 134 (1908) 198.
[63] G. Voronoï, J. Reine Angew. Math. 136 (1909) 67.
[64] A. Okabe, B. Boots, K. Sugihara, S.N. Chiu, Spatial Tessellations: Concepts and Applications of Voronoi Diagrams, John Wiley & Sons Ltd., Chichester, England, 2000.
[65] J.L. Finney, Proc. R. Soc. Lond. A 319 (1970) 479.
[66] R. Jullien, P. Jund, D. Caprion, D. Quitmann, Phys. Rev. E 54 (1996) 6035.
[67] L. Oger, A. Gervois, J.P. Troadec, N. Rivier, Phil. Mag. B 74 (1996) 177.
[68] P.L. Spedding, R.M. Spencer, Comput. Chem. Eng. 22 (1998) 247.
[69] P. Richard, L. Oger, J. Lemaître, L. Samson, N.N. Medvedev, Granular Matter 1 (1999) 203.
[70] R.Y. Yang, R.P. Zou, A.B. Yu, Phys. Rev. E 65 (2002) 041302.
[71] J.Q. Xu, R.P. Zou, A.B. Yu, Granular Matter 9 (2007) 455.
[72] A.V. Anikeenko, N.N. Medvedev, Phys. Rev. Lett. 98 (2007) 235504.
[73] T. Aste, T. Di Matteo, Phys. Rev. E 77 (2008) 021309.
[74] I. Schenker, F.T. Filser, L.J. Gauckler, T. Aste, H.J. Herrmann, Phys. Rev. E 80 (2009) 021302.
[75] C.B. Barber, D.P. Dobkin, H. Huhdanpaa, ACM Trans. Math. Softw. 22 (1996) 469.
[76] J.M.P.Q. Delgado, Heat Mass Transfer 42 (2006) 279.
[77] J.C. Giddings, Dynamics of Chromatography, Part 1: Principles and Theory, Marcel Dekker, New York, 1965.
[78] D.L. Koch, J.F. Brady, J. Fluid Mech. 154 (1985) 399.
[79] J. Bear, Dynamics of Fluids in Porous Media, Dover Publications, New York, 1988.
[80] S.G. Weber, P.W. Carr, in: P.R. Brown, R.A. Hartwick (Eds.), High Performance Liquid Chromatography, Wiley, New York, 1989, Chapter 1.
[81] A.L. Berdichevsky, U.D. Neue, J. Chromatogr. 535 (1990) 189.
[82] F. Gritti, G. Guiochon, Anal. Chem. 78 (2006) 5329.
[83] J.C. Giddings, Nature 184 (1959) 357.
[84] K. Miyabe, G. Guiochon, J. Sep. Sci. 26 (2003) 155.
[85] U. Tallarek, E. Bayer, G. Guiochon, J. Am. Chem. Soc. 120 (1998) 1494.
[86] P. Magnico, M. Martin, J. Chromatogr. 517 (1990) 31.
[87] J.H. Knox, J. Chromatogr. A 960 (2002) 7.
[88] J.H. Knox, J. Chromatogr. A 831 (1999) 3.
[89] R.A. Shalliker, B.S. Broyles, G. Guiochon, J. Chromatogr. A 888 (2000) 1.
[90] A. de Klerk, AIChE J. 49 (2003) 2022.
[91] G.E. Mueller, Powder Technol. 159 (2005) 105.
[92] J.J. van Deemter, F.J. Zuiderweg, A. Klinkenberg, Chem. Eng. Sci. 5 (1956) 271.
[93] K.M. Usher, C.R. Simmons, J.G. Dorsey, J. Chromatogr. A 1200 (2008) 122.
[94] J. Billen, P. Gzil, G.V. Baron, G. Desmet, J. Chromatogr. A 1077 (2005) 28.